Chemistry Europe
European Chemical Societies Publishing
Batteries & Supercaps

RESEARCH ARTICLE OPEN ACCESS

The Extent of Catholyte Gelation as a Critical Safety Factor in NMC-Based Solid-State Battery Design

Huw C. W. Parks[1,2] | Kai Ling Ng[2,3] | Hamish T. Reid[1] | Tom Risbridger[4] | Chris Vian[4] | Laura Perkins[4] | Paul R. Shearing[2,3] | James B. Robinson[1,2]

[1]Advanced Propulsion Lab, University College London, London, UK | [2]The Faraday Institution, Didcot, UK | [3]ZERO Institute, Holywell House, Osney Mead, University of Oxford, Oxford, UK | [4]Ilika PLC., Hampshire, UK

Correspondence: James B. Robinson (j.b.robinson@ucl.ac.uk)

Received: 16 February 2026 | **Revised:** 12 March 2026 | **Accepted:** 16 March 2026

Keywords: battery design | battery failure | battery safety | solid-state batteries

ABSTRACT

Solid-state batteries (SSBs) are considered a safer alternative to conventional lithium-ion batteries due to the replacement of flammable liquid electrolytes with solid electrolytes. However, many practical SSB designs incorporate liquid catholytes to reduce interfacial resistance at the cathode. The presence of liquid components introduces potential safety risks during failure events, yet the influence of catholyte formulation on cell safety remains poorly understood. In particular, the effect of catholyte gelation on thermal runaway behavior has not been experimentally evaluated. Here, we investigate the safety characteristics of QSSBs containing catholytes with varying degrees of gelation using nail penetration testing. Tests were performed on 2 Ah pouch cells at 100% SOC, with the surface temperature and video recorded throughout. Cells containing liquid catholytes underwent violent thermal runaway, reaching temperatures exceeding 400°C. In contrast, cells incorporating fully gelled catholytes showed no thermal runaway, with temperatures remaining below 25°C. Intermediate levels of catholyte gelation did not produce intermediate safety responses, with partial gelation failing to significantly mitigate failure severity. These results demonstrate that catholyte gelation can dramatically alter the thermal runaway behavior of QSSBs under internal short-circuit conditions and highlight the importance of electrolyte formulation when evaluating the safety of SSB systems.

1 | Introduction

Lithium-ion batteries have dominated the consumer electronics and automotive sectors for over three decades, with total worldwide production at nearly 4 TWh of energy storage in 2024, which is expected to double in the next 5–10 years [1, 2]. The performance of Li-ion cells in energy density, power density, cost, and availability has resulted in widespread deployment in electronic devices and electric vehicles (EVs) with increasingly challenging applications, including aerospace and aviation proposals [3]. In spite of their widespread deployment, safety concerns persist, particularly relating to thermal runaway (TR), which risks posing significant damage to human health and destruction of property [4–7]. While the occurrence of TR failure is rare, this issue has been highlighted to the general public through popular media, reinforcing the perception of poor safety performance in EV batteries [8–10].

Cathode active materials (CAMs) for lithium-ion and solid-state cells span a broad range of chemistries, each exhibiting distinct intrinsic safety characteristics. The two most commercially prominent classes are olivine-structured lithium iron phosphate (LFP) and layered mixed-metal oxides, typically comprising a stoichiometric mixture of nickel, manganese, and cobalt (NMC). From a safety perspective, LFP is widely regarded as the more thermally stable chemistry, though it remains capable of thermal runaway under sufficiently extreme abuse conditions [11, 12]. NMC, particularly high-nickel formulations, exhibits considerably more severe behavior, with the onset and intensity of thermal runaway being strongly dependent on the state of charge at the time of

abuse [13]. This disparity arises from two principal factors: first, NMC possesses a substantially higher gravimetric energy density at the cell level (LFP $\approx$ 170 Wh kg^{-1} theoretical maximum, NMC622 $\approx$ 250 Wh kg^{-1} in practice, with theoretical maxima approaching 280 Wh kg^{-1}), resulting in a greater total energy available for release during failure; and second, NMC undergoes oxygen evolution upon thermal decomposition, which can actively sustain and accelerate combustion. Comprehensive discussions of these comparative safety behaviors are provided in several established reviews [14–16].

Despite these safety concerns, NMC's superior energy density has driven its widespread adoption as a CAM of choice across many applications. The integration of a solid-state electrolyte may offer a viable pathway to mitigating these risks, potentially enabling the deployment of high-energy cathode materials alongside high-capacity anodes, such as lithium metal and silicon, within cell architectures that satisfy both energy density and safety requirements [17]. However, the safety benefits of solid-state electrolytes are not universal and can be strongly dependent on electrolyte chemistry, interfacial stability, and cell engineering; realizing these benefits, therefore, requires careful design consideration [18, 19]. Additionally, a holistic cell-level design approach is essential, encompassing cell casing geometry and integrated safety devices, on top of the electrode and electrolyte chemistries.

Currently, commercial liquid electrolyte technology is primarily composed of lithium salts and carbonate-based organic solvents, which are particularly flammable [20, 21]. The hazards associated with battery failure are acutely concerning, as mechanical damage to battery packs can result in the leakage of organic solvent electrolytes, which pose risks to both human health and the environment. In addition, the low ignition temperatures and poor thermal stability of these solvents increase the likelihood of thermal runaway during operation or following material degradation [22]. As we transition to higher energy density negative electrode materials, such as Li-metal, to improve the gravimetric energy densities of cells, conventional lithium-ion electrolytes become unsuitable, with strategies to enable these negative electrode developments requiring solid electrolytes (SE) suggested to facilitate this change [23].

Solid-state batteries (SSBs) offer significant safety advantages over conventional Li-ion alternatives [18, 19, 24, 25]. As discussed by Yu et al. [19], their lower thermodynamic energy reduces the likelihood of highly exothermic reactions under thermal stress, while solid electrolytes (SEs) help suppress lithium dendrite growth, a common failure mode in liquid electrolyte systems under low-temperature or high-rate conditions [26, 27]. The high thermal stability of SEs also raises the thermal runaway trigger temperature, though this alone may not prevent degradation of individual electrode components [28]. Despite these advantages, experimental safety data for SSBs and quasisolid-state batteries (QSSBs), particularly from industry-fabricated, high-energy-density pouch-cell prototypes, remain scarce. This reflects both the limited commercial availability of these devices at scales suitable for safety testing and the broad diversity of SE chemistries (ceramics, polymers, and hybrids), which resist generalization and often necessitate cell-specific characterization. This complexity is further compounded when liquid-phase components are introduced to form QSSBs [18].

While the safety of SSBs is widely perceived as being greater than their Li-ion counterparts, their rate performance, due to lower ionic conductivities through the SE, has been reported to be worse, impacting the performance of cells and hampering their commercial deployment [22]. To overcome these interfacial challenges, the addition of small amounts of liquid-containing catholyte has become common [29–31]. This is generally an organic solvent containing lithium salts, similar to a conventional liquid electrolyte, which is introduced at the interface of the solid electrolyte and the positive electrode to reduce interfacial resistance and stabilize the interface during cycling [19]. However, the presence of liquid components, which are often more flammable than SEs, could undermine the inherent safety typically associated with SSBs [32, 33].

The use of a liquid or gel catholyte has been motivated by previous studies, which report that chemically delithiated NMC acts as a strong oxidant toward the sulfide electrolyte, driving interfacial redox reactions that generate resistive decomposition products and cause progressive impedance growth [34]. Structurally, the anisotropic lattice strain associated with repeated lithiation cycles generates internal stresses that promote intergranular cracking and particle fragmentation [35–37]. In solid-state cells, unlike in liquid electrolyte systems, the electrolyte cannot infiltrate these cracks to maintain ionic pathways, meaning fractured regions become electrochemically isolated and create a self-reinforcing cycle of heterogeneous lithium transport and accelerating capacity loss [38]. While solid electrolytes can, in principle, mitigate some of these degradation pathways by mechanically constraining cathode particles, this benefit comes at the cost of higher interfacial resistance, which is precisely the limitation that has motivated the addition of liquid catholyte in many practical SSB designs [35, 38, 39]. Critically, the same cathode-electrolyte interfaces that govern electrochemical performance also represent a thermal hazard. Charged NMC/sulfide composite cathodes can undergo exothermic reactions under thermal abuse conditions, with interfacial heterogeneity in solid-state configurations potentially exacerbating rather than alleviating this risk [40].

Although all-solid-state batteries (ASSBs) have the potential to resolve these safety concerns, their performance, at present, is insufficient to ensure mass adoption. A deeper understanding of the trade-offs between safety and cell performance is crucial to position this technology as a viable option for automotive applications and the wider consumer market [41]. Several strategies have been proposed to address these safety challenges, including composite current collector designs [42], flame-retardant electrolyte additives [43], and ceramic-coated separators [44], each targeting distinct failure mechanisms. The use of gelled catholytes represents a further promising avenue, potentially offering a balance between the ionic conductivity required for rate performance and the reduced volatility and flammability needed to mitigate thermal runaway risk.

Nail penetration tests are a widely used method in the battery industry to evaluate the safety and thermal stability of batteries under severe mechanical abuse conditions [10, 45–47]. These tests simulate penetration by a conductive object that breaches the cell's protective casing and induces an internal short circuit, leading to intense localized Joule heating and rapid current flow. The resulting heat triggers successive exothermic reactions, accelerating temperature rise and ultimately leading to TR. Nail penetration is generally regarded as a more severe abuse condition than external thermal heating, as it combines mechanical damage, electrical shorting, and thermal decomposition. This type of

testing is critical because it replicates some of the most severe real-world hazards arising from high-impact accidents or manufacturing defects, which can lead to fires or explosions [48]. While the test is often perceived as extreme and may not represent the reality of the most common field failures, it is important to note that it is an industry standard test and a prerequisite for tests to pass existing safety standards, including the UL2580 and SAE J2464 [8, 10, 49]. It is also likely that this test will be retained in any future SSB testing standard, as it has the impact of fracturing the electrolyte and allowing short-circuiting to occur, something which may occur during a number of dynamic events,22 including vehicle impact.

While SSBs may offer compelling safety benefits, the incorporation of liquid catholyte introduces additional failure mechanisms that remain poorly characterized in the literature. Given that this approach is widely adopted by SSB manufacturers, it is critical to evaluate whether such hybrid configurations retain the inherent safety advantages of fully solid-state architectures. Here, the implications of this trade-off are systematically investigated using nail penetration testing to induce controlled internal short circuits across cells with varying catholyte formulations, with cell temperature and voltage monitored throughout each failure event. A distinct safety threshold is identified; fully gelled catholytes are shown to prevent thermal runaway, whereas liquid and partially gelled systems exhibit failure behavior comparable in severity to conventional liquid-electrolyte lithium-ion cells. This enhanced thermal stability in fully gelled systems is attributed to their reduced volatility and the capacity of the gel matrix to impede short-circuit-driven thermal propagation.

2 | Experimental Details

2.1 | Cell Details

Nail penetration testing was conducted on solid-state pouch cells (Ilika PLC, Hampshire, UK), which consisted of 12 alternating layers of NMC622 ($LiNi_{0.6}Mn_{0.2}Co_{0.2}O_2$) positive electrode and a silicon-containing graphite negative electrode, with a total cell capacity of ~2 Ah. The cells being assessed were a mix of cells containing a common electrolyte salt in a liquid catholyte and cells containing highly viscous gel catholytes; additional cells with intermediate levels of gelation were also tested. Cells were approximately 140 x 80 with 30 mm wide tabs located at top and bottom of the cell; see SI. Details of each cell and their catholyte composition can be found in Table 1. Further details of these cells are proprietary and not disclosed here.

2.2 | Nail Penetration

Failure testing was performed using MTI-TE901-U and MTI MSK800 (MTI Corp., CA, USA) with a Gamry Interface 1010E (Gamry Instruments, PA, USA) potentiostat connected to each cell via ring terminals. All cells were charged to 100% state-of-charge (SoC), equivalent to 4.2 V, with a constant current applied at a C-rate of C/5 (400 mA), and a constant voltage (CV) step applied at the top of charge until the current had reached 25% of the initial charging current (100 mA) to ensure 100% SoC had been reached. A 4 mm diameter stainless steel nail was used with a point angle of 45°. The nail was connected to a high-accuracy linear actuator that moved at 10 mm s^{-1} and remained in the pouch cell for 4 s before being removed. The chamber was at room temperature and open to atmospheric air; a slight negative vacuum was exhibited due to extraction system connected. Temperature was measured throughout the experiment using a Pico TC-08 thermocouple data logger (Pico Technology, St Neots, UK), where two N-type thermocouples were taped on top and two underneath the cell, placed approximately 2 cm from the nail entry hole between the positive and negative terminals. Images were taken using a 3.8K UHD camera (Dell UltraSharp Webcam WB7022, Dell Technologies) placed outside the explosion-proof chamber.

TABLE 1 | Table of cells tested and their catholyte composition.

Cell Number	Catholyte Composition
1	Liquid
2	Liquid
3	Gel
4	Gel
7	Medium Gel
8	Medium Gel
9	Medium Gel

3 | Results and Discussion

3.1 | Observations During Failure

Nail penetration testing was conducted on 4 SSBs, each comprising an NMC622 positive electrode and a graphite/silicon-blended negative electrode, separated by a proprietary solid electrolyte. Two cells contained a liquid catholyte (Cells 1 and 2), and two featured a fully gelled catholyte (Cells 3 and 4). Both catholytes consisted of a lithium-containing salt dissolved in organic solvents, differing only in the presence of a gelling agent. The inclusion of silicon in the negative electrode blend is notable, as silicon can undergo significant expansion and contraction during cycling, potentially influencing the mechanical and thermal stability of the solid electrolyte interphase (SEI) and solid electrolyte. Additionally, silicon-containing negative electrodes can exacerbate gas generation during TR due to electrolyte reduction reactions and the formation of lithium silicates, which, due to their exothermic formation reaction [50], are understood to significantly increase the temperatures reached during TR.

Figure 1 presents still images captured within the first 30 s post-penetration, highlighting distinctly differing behaviors between a cell with liquid and a cell containing fully gelled catholyte. In Cell 1 (Figure 1a–f), which contained a liquid catholyte, immediate production of a dense white vapor was observed upon nail penetration. This can be seen to be released from the puncture sites both above and below the cell. This phenomenon aligns with observations by Christensen et al. [51] in Li-ion pouch cells with NMC and graphite electrodes, where vapor production results from release of gaseous decomposition products of exothermic reactions, including the solid electrolyte interphase (SEI) decomposition at 90–120°C, electrolyte breakdown at 120–250°C,

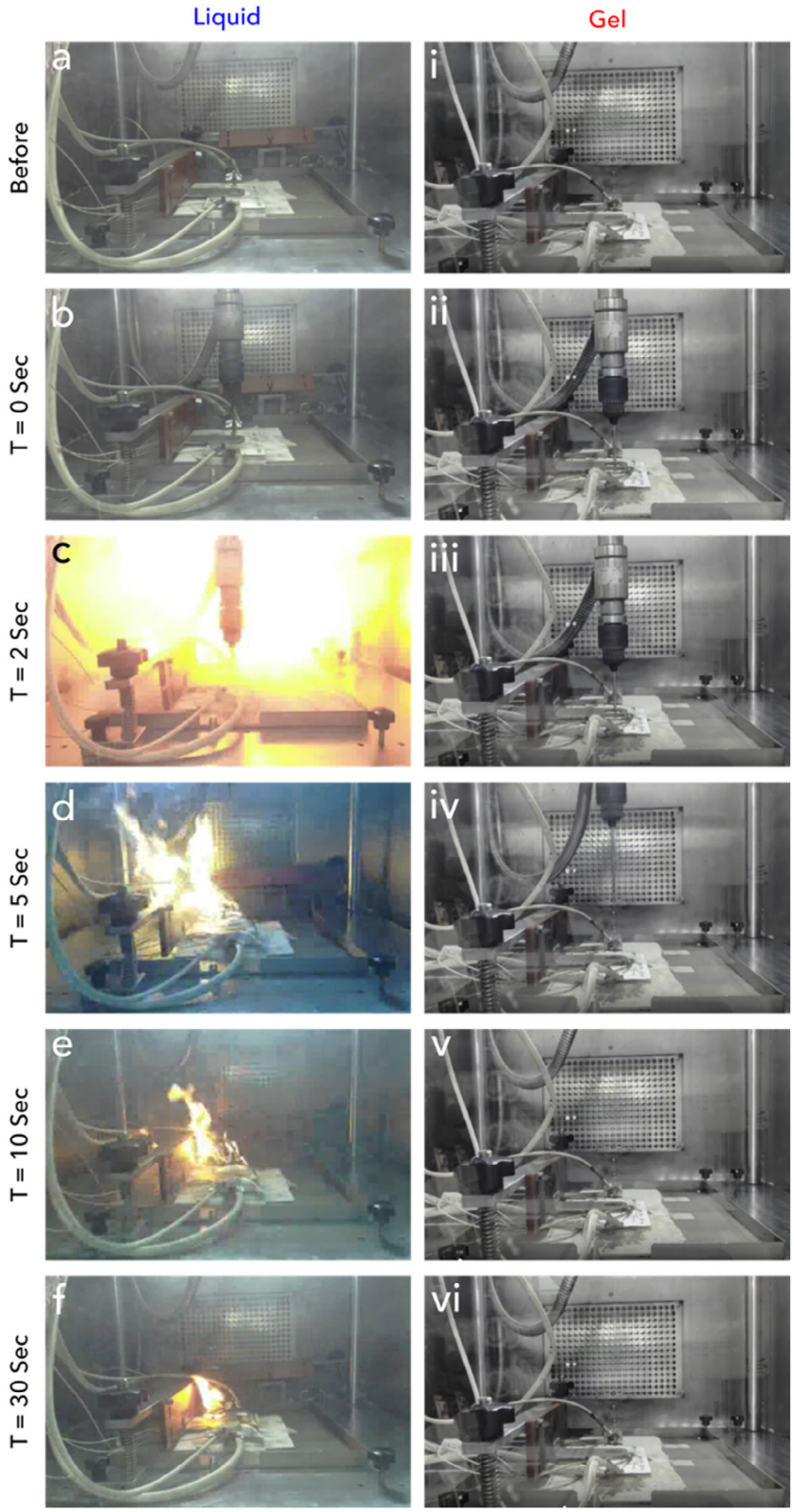

FIGURE 1 | Video stills during nail penetration testing for: (a–f) Cell 1 - Liquid catholyte, and (i–vi) Cell 3 - Gel catholyte, at the time stamps detailed, showing the divergent behavior of the two cell types, with the liquid cell (a–f) undergoing catastrophic thermal failure when compared to the benign response of the fully gelled cell (i–vi).

and positive electrode degradation >250°C. The rupture of the cell packaging, either by nail penetration or internal pressure buildup, causes the ingress of oxygen and moisture, accelerating exothermic reactions and promoting the onset of TR.

In Cell 1, a liquid-containing cell, rapid decomposition of the SEI and catholyte likely occurred due to Joule heating generated from current flow through internal short circuits and the conductive nail [52]. The vapor remained contained within the sealed

aluminum pouch for approximately 1 second before the pouch ruptured at the negative terminal; see SI. This can be attributed to pressure buildup from gas generation within the cell, which causes the negative terminal seal to fail, leading to a sudden release of flammable vapor. The failure at the negative electrode tab could be explained by the higher thermal conductivity of the negative electrode (primarily graphite) compared to the positive electrode (NMC), producing higher local temperatures, which cause additional gas generation and weakening of the cell seal, leading to failure. However, seal integrity may vary across the four seals in these cells, and thus, weaker seals may be breached before the negative seal gives way. Further analysis of seal integrity will be required to confirm this; however, this is outside the scope of this study.

The vapor produced in Cell 1, mainly originating from electrolyte decomposition, ignited immediately upon release, potentially triggered by sparks from hot fragments expelled through the ruptured seal (Figure 1c). This is further facilitated by the ingress of atmospheric oxygen and moisture. The resulting flame persisted for over 60 s, transitioning from bright yellow to white to orange as it cooled. This prolonged combustion may also be attributed to the ignition of the polymer-coated aluminum pouch material, particularly at the negative terminal end of the cell, where the highest temperatures were recorded. In contrast, prismatic or cylindrical cells, typically encased in steel, may exhibit reduced fire duration due to fewer flammable components. The geometry of the system may also impact the mechanism of failure, with the colocation of tabs at one side of the cell impacting the failure of the pouch, which may result in a directionally different result with tabs located on the same edge.

TR in liquid cells has been widely reported to generate gaseous products, including flammable species such as hydrogen (H_2), carbon monoxide (CO), and small hydrocarbons (e.g., ethylene [C_2H_4] and methane [CH_4]), as well as toxic species like hydrogen fluoride (HF), hydrogen cyanide (HCN), sulfur dioxide (SO_2), nitrogen dioxide (NO_2), and oxygen (O_2) from positive electrode decomposition, which is likely to have occurred in this scenario. However, since gas collection was not possible in this case, we rely on literature sources to speculate on the nature of these gases [51, 53]. The rapid ignition of the vapor cloud aligns with compositions observed in previous analyses of Li-ion battery failure events. Cell 2 (Liquid) can be found in the SI and shows a broadly similar response. However, without the presence of sparking, the vapor cloud fails to ignite, and vapor is continuously produced. The negative seal also remains intact in this experiment, despite the aggressive pouch swelling caused by vapor generation. This indicates some manufacturing variability in the seal robustness, which could significantly affect cell safety. If the seal prevents gas escape and limits oxygen access, vapor may fail to ignite externally, potentially leading to localized overheating and higher surface temperatures. Additional tests may be required to substantiate these claims further.

In stark contrast, Cell 3 (Figure 1i–vi), which contained the fully gelled catholyte, exhibited minimal response to nail penetration. No vapor release, cell expansion, or ignition was observed, indicating a significantly lower risk of TR compared to the cells with liquid catholytes. This suggests the gel catholyte may be more resistant to thermal decomposition or thermally more stable when compared to the liquid equivalent. The enhanced stability resulted in a lack of detectable vapor production, which suggests that either gas formation did not occur or was substantially reduced and that any of the gaseous products remained trapped within the cell without any venting, preventing their release and subsequent ignition. The enhanced thermal stability observed in the gel-based system may be attributed to the restricted movement of electrolyte, which limits the extent of short-circuit-driven decomposition reactions. It is worth noting that the anode, or negative electrode, contains silicon, which undergoes significant expansion upon charging (cells tested at fully charged state). The gel layer can accommodate this volume change, acting as a mechanical buffer that helps maintain electrode integrity. This can be supported by the X-ray CT volume rendering in the SI, which shows substantially less fracture of the electrode and SE layers in Cells 3 and 4 containing gel catholyte. Cell 4 follows the same trend observed here, with images available in the SI. It is also possible that the nail may not allow a full short circuit due to being coated by the gel during the penetrative event, reducing the conductivity of the nail during the test. However, this is speculative and requires additional testing of the electrolytes' electrical and coating properties; this is beyond the scope of this study.

The temperature and electrochemical data provide further insight into the observations made *via* video analysis. Each cell was set up with four thermocouples: two placed equally on the top of the cell between the nail penetration site and either terminal, and two in identical positions on the underside; see SI for schematic. Figure 2a–d presents the average temperature readings from these thermocouples, with full data available in the SI. As expected, the cells containing liquid catholyte (Cells 1 and 2) exhibited significantly higher surface temperatures, reaching peak values of 434°C and 344°C, respectively. In contrast, the fully gelled catholyte cells (Cells 3 and 4) remained relatively cool, with maximum recorded temperatures barely exceeding 25°C. A slight increase in temperature from room temperature to approximately 19.5°C indicates mild short-circuiting and Joule heating, but is insufficient to trigger the exothermic reactions that cause material decomposition and thermal runaway. The higher temperatures observed in liquid-based cells are likely driven by reactions between the catholyte and oxygen released from NMC decomposition, which produce much stronger exothermic behavior. Prior studies have shown that when the liquid content is reduced, and an in-situ solidified or quasisolid electrolyte is employed, the cathode-electrolyte reaction with NMC becomes less exothermic than with a fully liquid carbonate, mainly because the system moves away from rapid liquid–gas and liquid—solid combustion-type reactions [40]. This behavior is expected to be analogous to that of a gelled catholyte.

The more violent explosion and sustained fire in Cell 1 resulted in the highest recorded temperatures. Across these cells, the thermocouples located on the underside consistently registered higher temperatures than those on the top (see SI). This discrepancy likely arises because the lower thermocouples remain in direct contact with the thermally decomposing material, whereas the upper thermocouples lose contact due to inflation of the pouch material during failure. Additionally, a 20°C–40°C temperature differential was observed between the positive and negative terminals, with the negative terminal typically hotter. This thermal gradient may partially explain why the negative terminal was more likely to rupture; however, the variation in seal robustness between individual cells is also a contributing factor and may be resolvable with optimized manufacturing processes. The rupture of this seal enabled significant oxygen

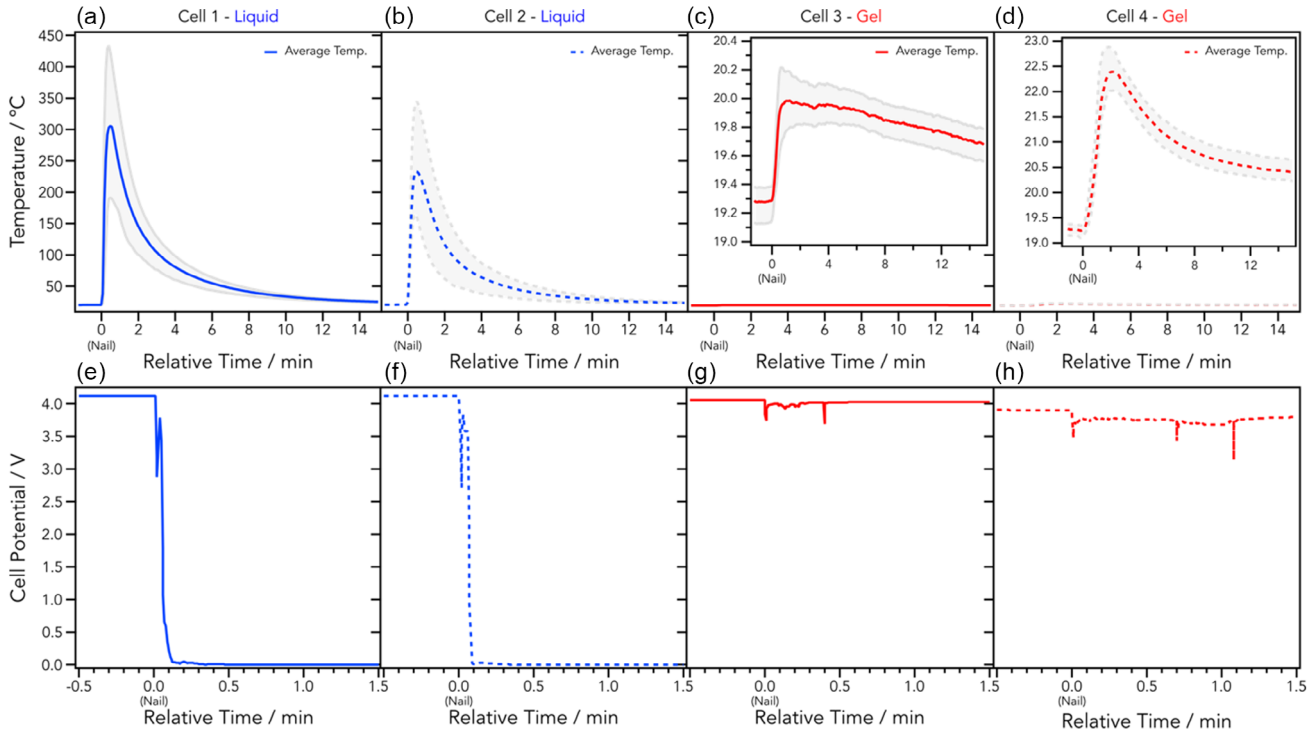

FIGURE 2 | (a–d) Average surface temperature analysis for first 15 min after nail penetration, with minimum and maximum temperature from 4 thermocouples attached to each cell with liquid or gel catholyte: (a) Cell 1 – liquid, (b) Cell 2 – liquid, (c) Cell 3 – gel, (d) Cell 4 - gel. Panel c and d have insets zoomed in on low-temperature region. (e–f) Voltage plots from (e) Cell 1, (f) Cell 2, (g) Cell 3, and (h) Cell 4 for the first 90 s after nail penetration.

ingress in Cell 1, which likely exacerbated combustion and sustained the fire.

The voltage profiles of each cell (Figure 2e–h) align with the temperature and video data, further confirming the differences in failure behavior between liquid and gel catholyte. Cells containing liquid catholyte exhibited catastrophic short circuits, while the gelled catholyte cells showed only minor voltage drops, maintaining voltages comparable to prepenetration levels. In the liquid-based cells, nail penetration caused an initial voltage drop, followed by a slight recovery, which occurred upon nail removal (after 4 s), before complete hard shorting. At this point, contact between electrodes likely resulted in a total voltage loss, coinciding with TR and mechanical failure. Conversely, the fully gelled cells exhibited only partial shorting, with minor voltage fluctuations but no full discharge. Both fully gelled cells maintained voltages above 3.5 V throughout the test and remained stable even upon subsequent discharge to 3.0 V. The retention of voltage suggests that the gel electrolyte physically separated the electrodes even when pierced, acting both as a physical spacer and a partially insulating layer, thereby restricting current flow and preventing a catastrophic short circuit.

While specific resistance values for the liquid and gelled catholytes remain proprietary, the high viscosity of the gelled medium is believed to provide a superior kinetic barrier. This rheological property may have actively suppressed lithium-ion flux across internal interfaces exposed during a penetration event, mitigating the risk of thermal runaway. In contrast, the liquid catholyte, which typically has a lower ignition temperature, has no such barrier and more readily facilitates TR and combustion. As mentioned above, this distinction is particularly noticeable in Cell 1, where, after nail penetration, the cell rapidly inflates, followed by rupture of the negative terminal seal that leads to a large vapor ejection. Moments after rupture, visible sparks are ejected, triggering immediate ignition. In Cell 2, where the vapor did not ignite, the gas venting obscured visibility, preventing direct observation of spark formation. However, as the seal remained intact, the combustion was prevented due to a lack of an ignition source and excess oxygen and water ingress, which can facilitate the combustion reactions. These observations require further systematic experimentation to understand further how seal integrity relates to cell safety.

3.2 | Postmortem Analysis

The loss of electrolyte and active materials is the consequence of the exothermic reactions that produce fumes containing ofgases and decomposed particles, which are expelled from the cell. Consequently, mass loss is a key indicator of cell safety during abuse testing and is one of the pass/fail criteria outlined in a number of international safety standards for lithium batteries [54, 55]. This metric reflects the loss of electrolyte and active materials through exothermic reactions that generate fumes containing gases and decomposed particles. The EUCAR hazard rating system provides a more nuanced assessment, with hazard levels 3 and 4 stipulating that no more than 50% of the original cell mass can be lost [56]. While none of the tested cells breached the 50% mass loss threshold, our results revealed stark differences in mass retention between catholyte types. Fully gelled catholyte cells (Cells 3 and 4) exhibited minimal mass loss of just 2.9% and 3.2%, respectively. By comparison, liquid catholyte cells (Cells 1

and 2) lost 43.6% and 36.0% of their mass due to vigorous fume production and ejection of electrolyte and electrode materials during nail penetration. While all cells remained below the 50% threshold, Cells 1 and 2 would qualitatively fail most standards, based on the presence of flames and violent gas ejection, illustrating that mass loss represents only one dimension of failure severity.

Visual inspection further highlights the difference in damage severity. As shown in Figure 3b,c, the liquid catholyte cells exhibited significant discoloration of the outer pouch, with yellow, brown, and black burn marks most prominent around the puncture site. In Cell 1, additional severe burning occurred near the negative seal, where flame ignition further damaged the pouch. Cell 2 also had significant discoloration but not the same charring as Cell 1, and thus, the discoloration occurred due to the significant heat of the rapidly decomposing active material during failure and not due to flames and ignition of the outer pouch material. By contrast, the gelled catholyte cells displayed minimal visual damage; aside from the puncture caused by the nail, there was no discoloration or visible burn damage, even in the immediate vicinity of the penetration site.

3.3 | Effect of Gel Strength

To further evaluate the effect of gel strength on cell safety during nail penetration abuse, three additional cells were assembled using a catholyte of intermediate/medium gelation extent, while all other components were kept constant. Although the manufacturer did not disclose specific formulation details, it was suggested that the viscosity of medium-gelled catholyte falls between the fully liquid formulation but remains less viscous than the fully gelled system. This intermediate state may have provided partial mitigation of TR severity by reducing electrolyte mobility or reduction in catholyte volatility while maintaining sufficient ionic conductivity for normal operation. All cells were charged to 4.2 V (100% SoC) and subjected to identical nail penetration testing protocols as before. Figure 4a–h presents video stills captured during nail penetration testing of the medium-gelled catholyte cells, alongside temperature and voltage data as before. Despite the altered catholyte, all cells experienced complete failure, marked by a rapid voltage drop to 0 V and extensive gassing, rupture, and material ejection, demonstrating that partial gelation alone is insufficient to prevent catastrophic thermal runaway.

Cell 7 exhibited immediate vapor generation upon penetration, with dense white vapor becoming visible within milliseconds postpenetration (see Data Repository section for full videos). This was followed by pronounced swelling of the cell pouch from significant internal gas generation during electrolyte decomposition and SEI breakdown, and within 2 s, the test chamber was filled with dense white vapor, demonstrating that the medium-strength gel provided insufficient resistance to prevent rapid gas evolution. Rupture of the cell's right-hand (right-hand refers to the view in Figure 4g) seal occurred after approximately 2 s, enabling the venting of hot fragments, mainly from the electrolyte components, which provided the ignition source for the surrounding vapor cloud.

The failure location in Cell 7 represents a notable deviation from the pattern observed in the liquid catholyte cells, where the negative terminal consistently ruptured first. In this instance, the right-hand seal failed first, again suggesting that manufacturing variability in seal integrity may play a more dominant role than the thermal gradient between terminals. Postmortem inspection revealed that while the negative seal had sustained significant impact, it remained mostly intact, indicating that the pressure buildup was sufficient to breach the weakest seal before a failure mechanism associated with thermal directionality could dominate at the negative terminal. Cell 8 displayed broadly similar behavior to Cell 7. The temperature and voltage data confirm that Cell 8 underwent complete TR with characteristics consistent with Cell 7. Additionally, postmortem visual inspection confirmed evidence of fire, including charring of the outer packaging.

In contrast, Cell 9 underwent substantial swelling and gas evolution but exhibited different failure characteristics (see Figure 4, right, and Figure 5b,d,f). While significant vapor generation occurred within the cell, all seals remained mostly intact throughout the test duration. No ignition or visible sparks were observed,

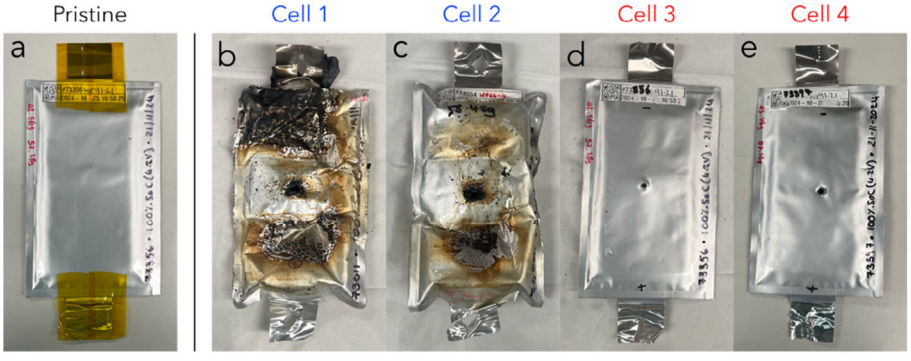

Liquid / Gel	Liquid	Liquid	Gel	Gel
Starting Mass (g)	57.38	57.44	57.28	57.15
End Mass (g)	32.36	36.78	55.62	55.34
Difference (g)	-25.02 (43.6%)	-20.66 (36.0%)	-1.66 (2.9%)	-11.81 (3.2%)

FIGURE 3 | (a) Image of Cell 3 in the as-shipped (pristine) state; (b–e) Images of each cell post nail penetration with relevant mass loss data tabulated underneath. (b) Cell 1, (c) Cell 2, (d) Cell 3, (e) Cell 4.

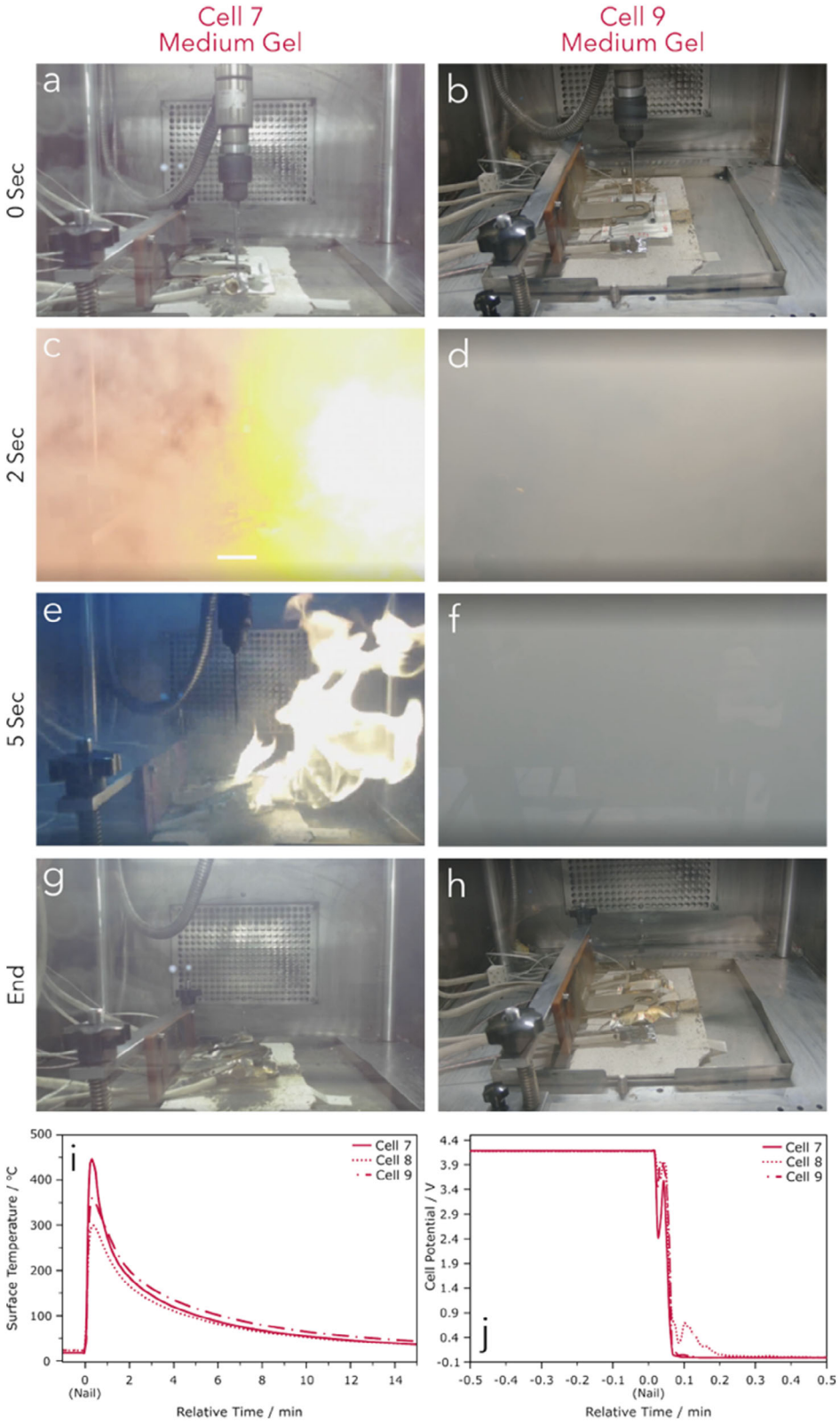

FIGURE 4 | Still from video captured at time points stated, for (a,c,e,g) Cell 7 and (b,d,f,h) Cell 9. (i) Average surface temperature for medium gel catholyte cells. (j) Voltage plots during nail penetration for medium gel catholyte cells.

despite clear evidence of internal decomposition reactions that cause the swelling. The voltage drop in Cell 9 was comparable to that of Cells 7 and 8, indicating that the short-circuit behavior was similar despite the different ignition response. The main reason for the absence of flame in Cell 9 may be the insufficient oxygen ingress to the ignition source due to maintained seal integrity; therefore, there is mild gas generation with the absence of expelled hot material and the suppression of an explosion/flames.

In terms of temperature profiles, each cell demonstrated rapid temperature increases. While peak temperatures varied between

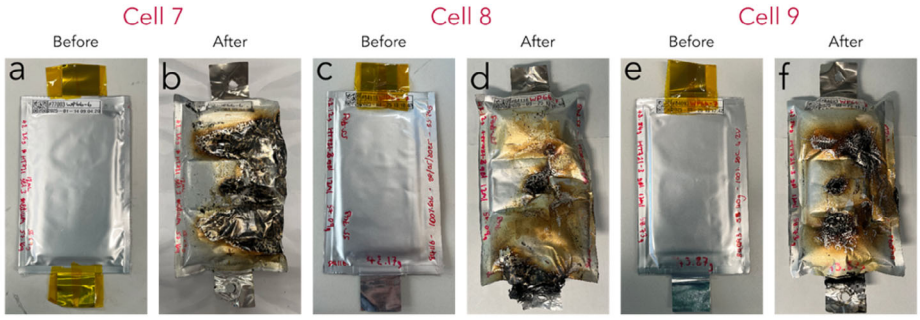

	Cell 7	Cell 8	Cell 9
Starting Mass (g)	55.09	55.74	57.40
End Mass (g)	34.86	33.58	41.43
Difference (g)	-20.23 (36.7%)	-22.16 (39.8%)	-15.97 (27.8%)

FIGURE 5 | (a,c,e) Images of Cell 7, 8, and 9 in the as-shipped (pristine) state. (b,d,f) Images of Cell 7, 8, and 9 post nail penetration with relevant mass loss data tabulated underneath.

cells, all demonstrated consistent heating rates, reaching maximum temperature within approximately 20 s. The average peak temperature for all three cells was between 300°C and 450°C, which would be typical for an all-liquid cell, again demonstrating the lack of safety advantage that only moderate gelling will achieve. It is also possible that reactions driven by oxygen evolution from NMC degradation play a role in compromising even intermediately gelled catholytes, contributing to the complete and catastrophic failure of individual cells. Voltage profiles again suggest complete failure with rapid short-circuiting to 0 V in a matter of milliseconds.

Figure 5 presents the postmortem appearance of Cells 7, 8, and 9 following nail penetration testing. As previously discussed, Cells 1 and 2 (100% liquid catholyte) exhibited severe external damage, including dark charring, extensive discoloration, and pouch rupture near both the puncture site and electrode seals, associated with high mass losses (43.6% and 36.0%, respectively). We observe broadly the same here; Cell 7 underwent violent failure with significant swelling, seal rupture, ignition, and hot material ejection. The resulting external damage closely resembled that of Cell 1, with severe charring and discoloration throughout the pouch surface.

Cell 8 also experienced flame ignition and rupture; the most intense charring occurred around the positive electrode seal rather than the typical negative terminal location. This unusual pattern suggests possible manufacturing-related asymmetry, such as electrode misalignment or variation in seal thickness, creating a weaker positive seal that failed preferentially. Cell 9, while avoiding ignition and excessive rupture, exhibited pronounced swelling and moderate surface discoloration. Despite the absence of flame, the cell experienced 27.8% mass loss,

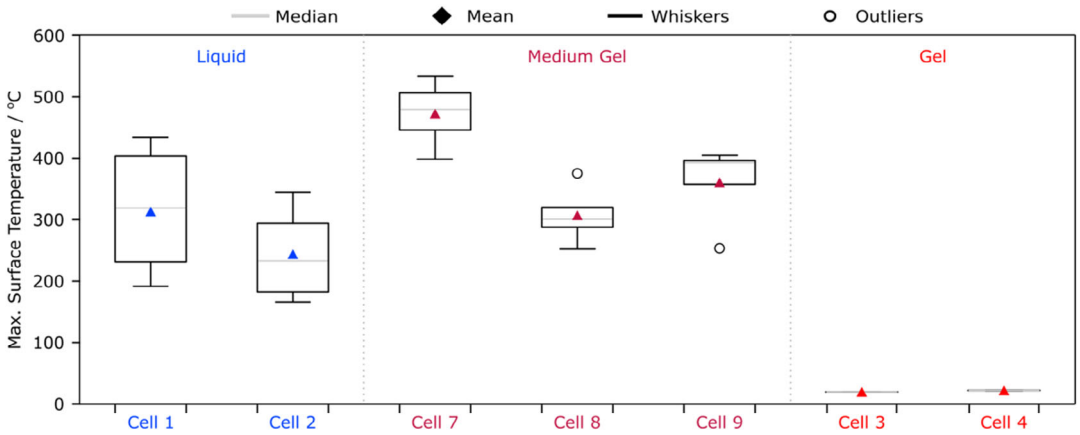

Cell Number	Catholyte Type	Maximum Surface Temperature / °C	Fire?	Burst Seals?	Final Voltage / V
Cell 1	Liquid	434.0	Yes	Neagtive, Left	0
Cell 2	Liquid	344.3	No	Negative, Positive	0
Cell 3	Gel	20.2	No	No	4.03
Cell 4	Gel	22.9	No	No	3.82
Cell 7	Medium Gel	533.2	Yes	Right	0
Cell 8	Medium Gel	375.2	Yes	Positive	0
Cell 9	Medium Gel	404.8	No	No	0

FIGURE 6 | (Top) Box and whisker plot of surface temperature from the four thermocouples attached to each cell, for each cell analyzed. (Bottom) Tabulated data for cell failure identifiers.

indicating substantial internal gas generation and pressure buildup. This indicates that volatile species were likely vented gradually or through minor leakage pathways, while the seals maintained enough integrity to delay or prevent ignition through limiting the ingress of atmospheric oxygen. Cells 7 and 8 lost 36.7% and 39.8% of their original mass, which appears to be typical for these cells if they suffer seal rupture and TR.

Figure 6 compares maximum surface temperatures recorded across all cells, revealing distinct performance categories based on catholyte type. The liquid catholyte cells (Cells 1 and 2) reached peak temperatures of 434°C and 344°C, respectively, consistent with thermal runaway temperatures typically observed in conventional lithium-ion cells during nail penetration testing. Increasing gelation to a medium level failed to provide meaningful safety improvements. The medium-gelled cells (Cells 7–9) achieved similar peak temperatures ranging from 284°C to 533°C, demonstrating that partial gelation offers no improvement compared to cells containing a liquid catholyte. All medium-gelled cells experienced complete voltage collapse and exhibited failure behaviors comparable to the liquid catholyte systems.

However, a dramatic safety improvement was observed with fully gelled catholytes. Cells 3 and 4 maintained surface temperatures below 25°C throughout testing. This temperature stability coincided with only minor voltage drops, with both cells maintaining voltages above 3.5 V for hours after testing. These results suggest that complete gelation creates a critical threshold effect, preventing hard short circuits between electrodes and significantly reducing catholyte volatility. The severity of failure events further emphasizes the threshold nature of gelation effects. Among the five liquid-containing cells tested, three experienced catastrophic failure with ignition, which coincided with seal rupture. In contrast, both fully gelled cells remained stable with no observable failure indicators. The ignition events consistently correlated with major seal ruptures, and in the most severe cases, multiple seals failed simultaneously.

The results demonstrate that quasisolid-state batteries (QSSB) or solid-state batteries employing interfacial agents may exhibit failure behaviors as severe as their liquid electrolyte counterparts when gelation levels fall below a critical threshold. The binary nature of the safety performance observed here, with complete protection at full gelation but minimal improvement at intermediate levels, indicates that catholyte design must prioritize complete electrolyte immobilization rather than incremental viscosity increases for potential ion mobility.

4 | Conclusion

This work demonstrates that the safety benefits of solid-state batteries containing NMC622 are dependent on complete catholyte gelation. Through systematic nail penetration testing, we found a sharp safety threshold. Gelled catholyte may have offered combined mechanical and electrical protection during nail penetration. The fully gelled catholytes prevented thermal runaway entirely, maintaining temperatures below 25°C with minimal voltage drop and under 3.5% mass loss. In contrast, the liquid and partially gelled catholytes exhibit catastrophic failures comparable to conventional lithium-ion cells, with temperatures exceeding 400°C, mass losses of 36–44%, and violent ignition events. The binary nature of this threshold is particularly significant. Medium-gel catholytes offered little obvious safety improvement over liquid systems, showing that incremental viscosity increases may not simply be enough. This challenges the common assumption that solid-state architectures inherently provide superior safety. In fact, our results show that hybrid systems incorporating mobile catholyte components can reintroduce the hazards that solid-state technology was designed to eliminate.

These findings provide important design guidance. Catholyte formulations must prioritize complete electrolyte gelation rather than performance-driven compromises that maintain partial fluidity if they are seeking to manufacture QSSBs with a nonsolid interfacial resistance reduction medium. As manufacturers develop quasisolid-state batteries to address interfacial resistance challenges, our results make it clear that catholyte gelation might not be treated as a tunable parameter for balancing performance and safety. Full gelation is a critical safety requirement in this cell architecture. Achieving the promised safety advantages of solid-state technology in commercially viable cells requires uncompromising attention to catholyte rheology and volatility suppression.

Data Repository

Full video data files under CC by 4.0 license can be found at: https://doi.org/10.5522/04/29669153.v1.

Acknowledgments

The authors would like to thank the Faraday Institution for funding this work through the Sprint Project FIRG073 and the SAFEBATT project (FIRG086). P.R.S and J.B.R would also like to acknowledge the Faraday Institution (Faraday.ac.uk; EP/S003053/1) for funding the energy storage work at the Advanced Propulsion Lab, UCL, and the Department of Engineering Sciences, University of Oxford (FIRG083). P.R.S also acknowledges the Royal Academy of Engineering Chair in Emerging Technologies (CiET1718\59). H.T.R, P.R.S, and J.B.R would like to acknowledge the Aerospace Technology Institute for their funding of the CEBD programme *via* Innovate UK (10050803). Finally, we would like to thank Ilika plc for their provision of cells for the experiments conducted in this work.

Funding

This study was supported by the Faraday Institution (FIRG073, FIRG086, FIRG083), Innovate UK (10050803), and the Royal Academy of Engineering (CiET1718\59).

Conflicts of Interest

The authors declare no conflicts of interest.

References

1. J. Fleischmann, M. Hanicke, E. Horetsky, et al., *Battery 2030: Resilient, sustainable, and circular* (2023).

2. R. F. H. Hernandha, "Research, Development, and Innovation Insights for Solid-State Lithium Battery: Laboratory to Pilot Line Production," *Discover Electrochemistry* 2 (2025).

3. H. T. Reid, G. Singh, E. Palin, et al., "Key Considerations for Cell Selection in Electric Vertical Take Off and Landing Vehicles: A Perspective," *EES Batteries* 1 (2025): 227–241.

4. D. P. Finegan, M. Scheel, J. B. Robinson, et al., "In-Operando High-Speed Tomography of Lithium-Ion Batteries during Thermal Runaway," *Nature Communications* 6 (2015): 6924.

5. Z. Chen, R. Xiong, J. Lu, and X. Li, "Temperature Rise Prediction of Lithium-Ion Battery Suffering External Short Circuit for All-Climate Electric Vehicles Application," *Applied Energy* 213 (2018): 375–383.

6. X. Feng, M. Ouyang, X. Liu, L. Lu, Y. Xia, and X. He, "Thermal Runaway Mechanism of Lithium Ion Battery for Electric Vehicles: A Review," *Energy Storage Materials* 10 (2018): 246–267.

7. D. H. Doughty and E. P. Roth, "A General Discussion of Li Ion Battery Safety," *The Electrochemical Society Interface* 21 (2012): 37.

8. Y. Chen, Y. Kang, Y. Zhao, et al., "A Review of Lithium-Ion Battery Safety Concerns: The Issues, Strategies, and Testing Standards," *Journal of Energy Chemistry* 59 (2021): 83–99.

9. J. Wen, Y. Yu, and C. Chen, "A Review on Lithium-Ion Batteries Safety Issues: Existing Problems and Possible Solutions," *Materials Express* 2 (2012): 197–212.

10. J. Jaguemont and F. Bardé, "A Critical Review of Lithium-Ion Battery Safety Testing and Standards," *Applied Thermal Engineering* 231 (2023): 121014.

11. Y. Zhang, S. Cheng, W. Mei, et al., "Understanding of Thermal Runaway Mechanism of LiFePO4 Battery in-Depth by Three-Level Analysis," *Applied Energy* 336 (2023): 120695.

12. T. Sun, L. Wang, D. Ren, et al., "Thermal Runaway Characteristics and Modeling of LiFePO4 Power Battery for Electric Vehicles," *Automotive Innovation* 6 (2023): 414–424.

13. K. O. A. Amano, S.-K. Hahn, R. Tschirschwitz, T. Rappsilber, and U. Krause, "An Experimental Investigation of Thermal Runaway and Gas Release of NMC Lithium-Ion Pouch Batteries Depending on the State of Charge Level," *Batteries* 8 (2022): 41.

14. W. Li, J. Wang, C. Sun, et al., "Comparison on Thermal Runaway and Critical Characteristics of Cylindrical Lithium-Ion Batteries: A Review," *ACS Chemical Health & Safety* 32 (2025): 133–156.

15. M. Brand, S. Gläser, J. Geder, et al., In *2013 World Electric Vehicle Symposium and Exhibition (EVS27)*, (IEEE, 2013), 1–9.

16. S. Ohneseit, P. Finster, C. Floras, et al., "Thermal and Mechanical Safety Assessment of Type 21700 Lithium-Ion Batteries with NMC, NCA and LFP Cathodes–Investigation of Cell Abuse by Means of Accelerating Rate Calorimetry (ARC)," *Batteries* 9 (2023): 237.

17. Z. Wang, B. Bhargava, N. B. Johnson, et al., "Early-Stage Thermal Safety Evaluation of the NMC811/LLZO/Li Solid-State Battery Chemistry Using Calorimetry and Characterization Methods," *ACS Applied Materials & Interfaces* 17 (2025): 59289–59300.

18. A. M. Bates, Y. Preger, L. Torres-Castro, K. L. Harrison, S. J. Harris, and J. Hewson, "Are Solid-State Batteries Safer than Lithium-Ion Batteries?," *Joule* 6 (2022): 742–755.

19. X. Yu, R. Chen, L. Gan, H. Li, and L. Chen, "Battery Safety: From Lithium-Ion to Solid-State Batteries," *Engineering* 21 (2023): 9–14.

20. G. E. Blomgren, "Liquid Electrolytes for Lithium and Lithium-Ion Batteries," *Journal of Power Sources* 119 (2003): 326–329.

21. S. S. Zhang, "A Review on Electrolyte Additives for Lithium-Ion Batteries," *Journal of Power Sources* 162 (2006): 1379–1394.

22. C. Li, Z. Wang, Z. He, et al., "An Advance Review of Solid-State Battery: Challenges, Progress and Prospects," *Sustainable Materials and Technologies* 29 (2021): e00297.

23. C. Wang, C. Yang, and Z. Zheng, "Toward Practical High-Energy and High-Power Lithium Battery Anodes: Present and Future," *Advanced Science* 9 (2022): 2105213.

24. M. Pasta, D. Armstrong, Z. L. Brown, et al., "2020 Roadmap on Solid-State Batteries," *Journal of Physics: Energy* 2 (2020): 032008.

25. F. Salk, S. Schuhmann, P. Heugel, F. Klein, J. Tübke, and I. C. T. Fraunhofer, In *International Battery Safety Workshop 2023* (2023).

26. Q. Li, G. Liu, H. Cheng, Q. Sun, J. Zhang, and J. Ming, "Low-Temperature Electrolyte Design for Lithium-Ion Batteries: Prospect and Challenges," *Chemistry–A European Journal* 27 (2021): 15842–15865.

27. R. E. Owen and J. Robinson, *Electrochemical Society Meeting Abstracts prime2024* (The Electrochemical Society, Inc, 2024), 771.

28. W. D. Richards, L. J. Miara, Y. Wang, J. C. Kim, and G. Ceder, "Interface Stability in Solid-State Batteries," *Chemistry of Materials* 28 (2016): 266–273.

29. Y. Zhang, B. Gou, Y. Li, et al., "Integration of Gel Polymer Electrolytes with Dry Electrodes for Quasi-Solid-State Batteries," *Chemical Engineering Journal* 498 (2024): 155544.

30. L. Mazzapioda, A. Tsurumaki, G. Di Donato, H. Adenusi, M. A. Navarra, and S. Passerini, "Quasi-Solid-State Electrolytes - Strategy Towards Stabilizing Li|Inorganic Solid Alectrolyte Interfaces in Solid-State Li Metal Batteries," *Energy Materials* 3 (2023): 1–3025.

31. Y. Yu, X. Liu, Z. Tian, et al., "Safety Assessment of Large-Format Quasi-Solid-State Lithium-Ion Batteries," *Advanced Energy Materials* 16 (2025): e04346.

32. S. Chen, Q. Peng, Z. Wei, et al., "Revealing the Quasi-Solid-State Electrolyte Role on the Thermal Runaway Behavior of Lithium Metal Battery," *Energy Storage Materials* 70 (2024): 103481.

33. C. Bao, C. Zheng, J. Zhang, et al., "A High Performance Fireproof Quasi-Solid-State Electrolyte Enabled by Multi-Phase Synergistic Mechanism," *Energy Storage Materials* 68 (2024): 103362.

34. X. Hu, Z. Zhao, Y. Zhao, et al., "Interfacial Degradation of the NMC/Li_6PS_5Cl Composite Cathode in All-Solid-State Batteries," *Journal of Materials Chemistry A* 12 (2024): 3700–3710.

35. H. Chen, H. H. Wu, and C. C. Li, "Solid Electrolyte-Driven Suppression of H2–H3 Phase Transition in Ni-Rich Cathodes for Stable High-Voltage Cycling," *Current Opinion in Solid State & Materials Science* 39 (2025): 101245.

36. H. Parks, M. Jones, A. Wade, et al., "Non-Linear Damage Response to Voltage Revealed by Operando X-ray Tomography in Polycrystalline NMC811," *EES Batteries* 3 (2025).

37. H. C. W. Parks, A. M. Boyce, A. Wade, et al., "Direct Observations of Electrochemically Induced Intergranular Cracking in Polycrystalline NMC811 Particles," *Journal of Materials Chemistry A* 11 (2023): 21322–21332.

38. X. Zheng, Z. Xue, H. Hao, et al., "*Unravelling Electro-Chemo-Mechanical Interplay in Layered Oxide Cathode Degradation in Solid-State Batteries*," *Science Advances* 11 (2025): eady7189.

39. L. Yang, J. Zhang, W. Xue, et al., "Anomalous Thermal Decomposition Behavior of Polycrystalline $LiNi_{0.8}Mn_{0.1}Co_{0.1}O_2$ in PEO-Based Solid Polymer Electrolyte," *Advanced Functional Materials* 32 (2022): 2200096.

40. L. Gan, X. Xu, X. Yu, and H. Li, "Assessing the Thermal Runaway Characteristics of Solid-State Lithium Batteries Based on Thermochemical Reaction Properties at Material Level," *Energy Storage Materials* 78 (2025): 104223.

41. X. Rui, D. Ren, X. Liu, et al., "Distinct Thermal Runaway Mechanisms of Sulfide-Based All-Solid-State Batteries," *Energy & Environmental Science* 16 (2023): 3552–3563.

42. Z. Liu, Y. Dong, X. Qi, et al., "Stretchable Separator/Current Collector Composite for Superior Battery Safety," *Energy & Environmental Science* 15 (2022): 5313–5323.

43. C.-A. Chen and C.-C. Li, "Microencapsulating Inorganic and Organic Flame Retardants for the Safety Improvement of Lithium-Ion Batteries," *Solid State Ionics* 323 (2018): 56–63.

44. A. Gogia, Y. Wang, A. K. Rai, R. Bhattacharya, G. Subramanyam, and J. Kumar, "Binder-Free, Thin-Film Ceramic-Coated Separators for Improved Safety of Lithium-Ion Batteries," *ACS Omega* 6 (2021): 4204–4211.

45. S. Tobishima, K. Takei, Y. Sakurai, and J. Yamaki, "Lithium Ion Cell Safety," *Journal of Power Sources* 90 (2000): 188–195.

46. T. Ma, L. Chen, S. Liu, et al., "Mechanics-Morphologic Coupling Studies of Commercialized Lithium-Ion Batteries under Nail Penetration Test," *Journal of Power Sources* 437 (2019): 226928.

47. J. Diekmann, S. Doose, S. Weber, S. Münch, W. Haselrieder, and A. Kwade, "Development of a New Procedure for Nail Penetration of Lithium-Ion Cells to Obtain Meaningful and Reproducible Results," *Journal of the Electrochemical Society* 167 (2020): 090504.

48. B. Mao, H. Chen, Z. Cui, T. Wu, and Q. Wang, "Failure Mechanism of the Lithium Ion Battery during Nail Penetration," *International Journal of Heat and Mass Transfer* 122 (2018): 1103–1115.

49. X. Lai, J. Yao, C. Jin, et al., "A Review of Lithium-Ion Battery Failure Hazards: Test Standards, Accident Analysis, and Safety Suggestions," *Batteries* 8 (2022): 248.

50. Y.-S. Su, K.-C. Hsiao, P. Sireesha, and J.-Y. Huang, "Lithium Silicates in Anode Materials for Li-Ion and Li Metal Batteries," *Batteries* 8 (2022): 2.

51. P. A. Christensen, Z. Milojevic, M. S. Wise, et al., "Thermal and Mechanical Abuse of Electric Vehicle Pouch Cell Modules," *Applied Thermal Engineering* 189 (2021): 116623.

52. T. Yokoshima, D. Mukoyama, F. Maeda, et al., "Direct Observation of Internal State of Thermal Runaway in Lithium Ion Battery during Nail-Penetration Test," *Journal of Power Sources* 393 (2018): 67–74.

53. T. Yoon, M. S. Milien, B. S. Parimalam, and B. L. Lucht, "Thermal Decomposition of the Solid Electrolyte Interphase (SEI) on Silicon Electrodes for Lithium Ion Batteries," *Chemistry of Materials* 29 (2017): 3237–3245.

54. UN. Committee of Experts on the Transport of Dangerous Goods UN, *Committee of Experts on the Transport of Dangerous Goods and on the Globally Harmonized System of Classification and Labelling of Chemicals, Recommendations on the Transport of Dangerous Goods.: Manual of Tests and Criteria* (UN, 2019).

55. TUV SUD, *tuvsud-lithium-battery-testing-under-UN-DOT-38-3*, (2019), https://www.tuvsud.com/en-us/resource-centre/white-papers/lithium-battery-testing.

56. C. Ashtiani, "Analysis of Battery Safety and Hazards' Risk Mitigation," *Electrochemical Society Transactions* 11, no. 212 (2008): 1.

Supporting Information

Additional supporting information can be found online in the Supporting Information section.